Electronic Supplementary Information

Highly Crystalline Ramsdellite as a Cathode Material for Near-Neutral Aqueous MnO$_2$/Zn Batteries

Ivan Stoševski,[a] Arman Bonakdarpour, [*a] Faye Cuadra [a] and David P. Wilkinson [*a]

[a]Department of Chemical and Biological Engineering and the Clean Energy Research Center, University of British Columbia, 2360 East Mall, Vancouver, BC, V6T 1Z3, CANADA

Experimental Methods

Synthesis of MnO$_2$ and Electrochemical Measurements

Three grams of LiMn$_2$O$_4$ powder (BE-30, NEI Corporation) was mixed with 15 ml of 2.5 M H$_2$SO$_4$ (96.8 %, Sigma-Aldrich, LOT#SHBG0974V) and stirred at 80 °C for 2.5 hours. The powder was washed with ultra-pure water (18.2 MΩ cm, Milli-Q Integral 5, Fisher Scientific International Inc.) four times, centrifuged and then was dried overnight at 80 °C in an oven (VDO-23i, Hydrion Scientific Instruments).

Cathode electrodes were prepared by mixing the synthesized MnO$_2$ powder, carbon black (Vulcan XC72R, Cabot Corporation) and polyvinylidene fluoride (EQ-Lib-PVDF, MTI Corporation) in a mass ratio of 7 : 2 : 1, dispersed in 1.4 g of n-methyl-2-pyrrolidone (EQ-Lib-NMP, MTI Corporation) and deposited onto carbon paper (Toray TGP-H-120, Fuel Cell Earth). The electrodes were dried overnight at 80 °C in an oven. The MnO$_2$ mass loading in the electrode was about 2 – 4 mg cm^{-2}.

Electrochemical measurements were conducted in coin cell hardware (CR2032, MTI Corporation). A bilayer cellophane film/nonwoven polyimide paper (NWP150, Neptco) and zinc foil (0.13 mm thick, 31050, Dexmet Corporation) were employed as the separator and anode, respectively. The separator was swollen with 2 M ZnSO$_4$ (99%, Anachemia) or 1.5 M Zn(CF$_3$SO$_3$)$_2$ (98 %, Acros Organics) aqueous solutions or with 0.5 M Zn(CF$_3$SO$_3$)$_2$ acetonitrile (99.8 %, Acros Organics) based solution. The discharge/charge cycles were performed by a computer-controlled Maccor 4300 battery analyzer. The cells were cycled with the following protocol: i) galvanostatic discharge to 1.1 V for ZnSO$_4$ or to 0.8 V for Zn(CF$_3$SO$_3$)$_2$ electrolyte, ii) galvanostatic charge to 1.9 V, and iii) potentiostatic charging at 1.9 V for 20 min. All measurements were performed at room temperature (~21°C).

Physical and Chemical Characterizations

Inductively coupled plasma - optical emission spectrometry (ICP-OES) measurements were performed using a Varian 725ES Optical Emission Spectrometer. The samples were prepared for analysis by dissolving electrode material in the concentrated nitric acid, drying to a volume less than 100 µL and addition of 2 % HNO$_3$ solution to a final volume of 10 mL.

For all other measurements, materials were characterized in powder form. The cycled samples were removed from current collectors, washed, and ground to a fine powder prior to measurements. X-Ray Diffraction (XRD) and Thermogravimetric (TGA) measurements were

performed using a Bruker D2 Phaser diffractometer (Cu Kα radiation source) and a TA Instruments Q500, respectively. TGA measurements comprised of initial heating at a temperature of 80 $^{\circ}$C for 30 minutes to remove any adsorbed water, followed by a heating step using a thermal rate of 2 $^{\circ}$C min^{-1} up to 600 $^{\circ}$C. X-ray Photoelectron Spectroscopy (XPS) measurements were conducted with an Omicron & Leybold MAX200 instrument.

Estimation of the extent of microtwinning

Chabre et al.[1] has proposed several methods for estimation of microtwinning (T_w) in the ramsdellite grains. The approach used in this paper is based on the following equation:

$$T_w(\%) = 871\frac{a}{2c} - 1409$$

The equation is derived by calculating the ratio of the ramsdellite lattice parameters, $a/2c$ from the (a^*,c^*) reciprocal plane assuming different amounts of twinning. For example, natural ramsdellite is considered to have a T_w value equal to 0, while the fully twinned structure (T_w = 100 %) gives $a/2c$ the value of $\sqrt{3}$.
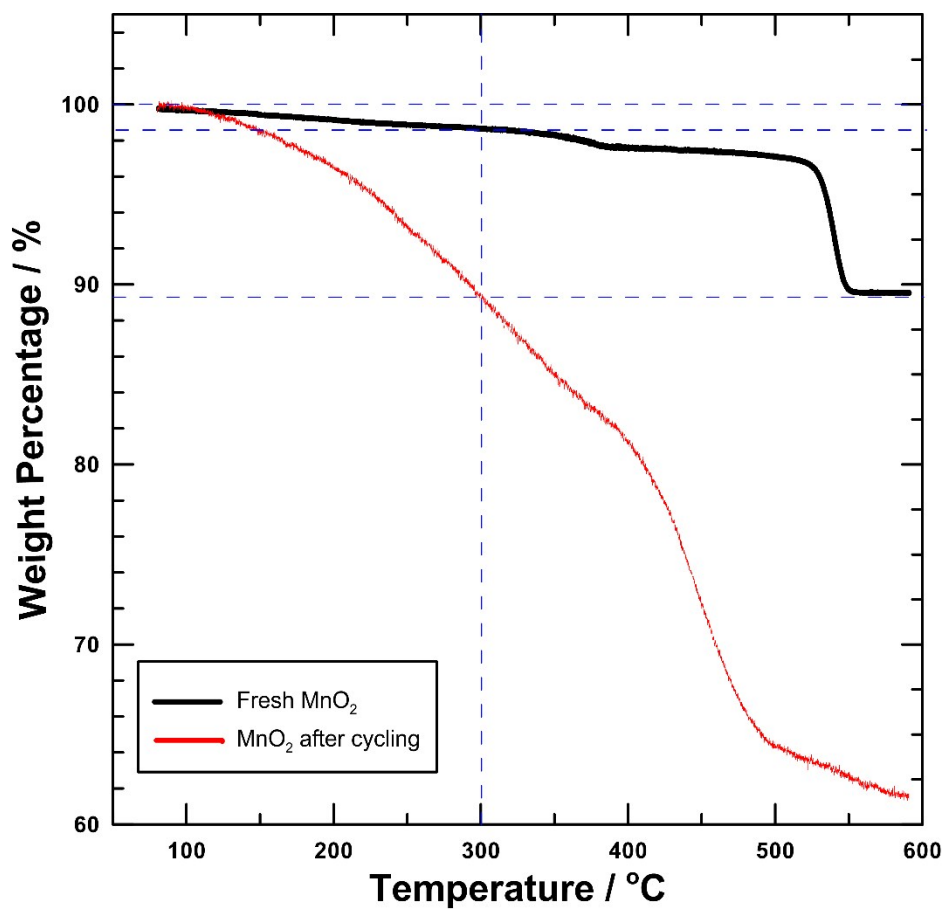
**Figure S1**. Weight percentage of the freshly synthesized and cycled MnO_2 samples vs. temperature.
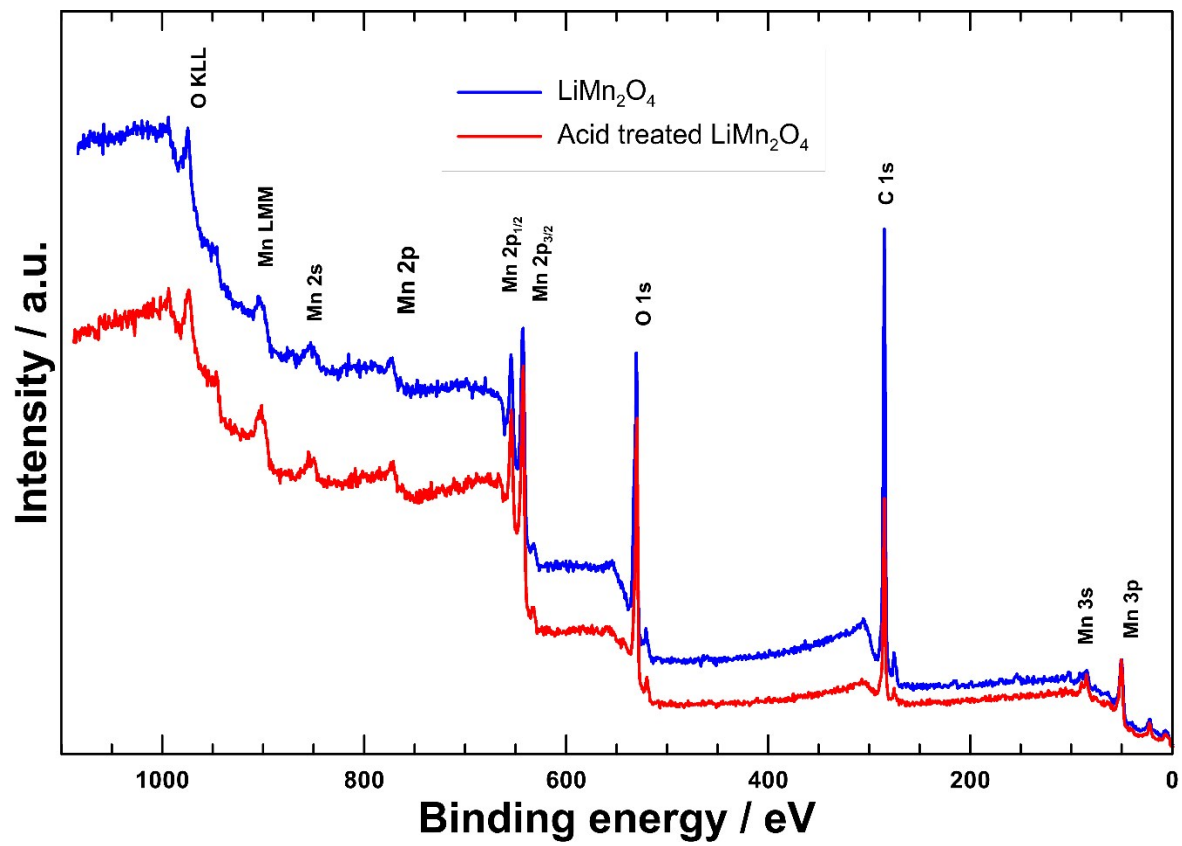
Figure S2. XPS spectra of LiMn$_2$O$_4$ precursor and the synthesized MnO$_2$
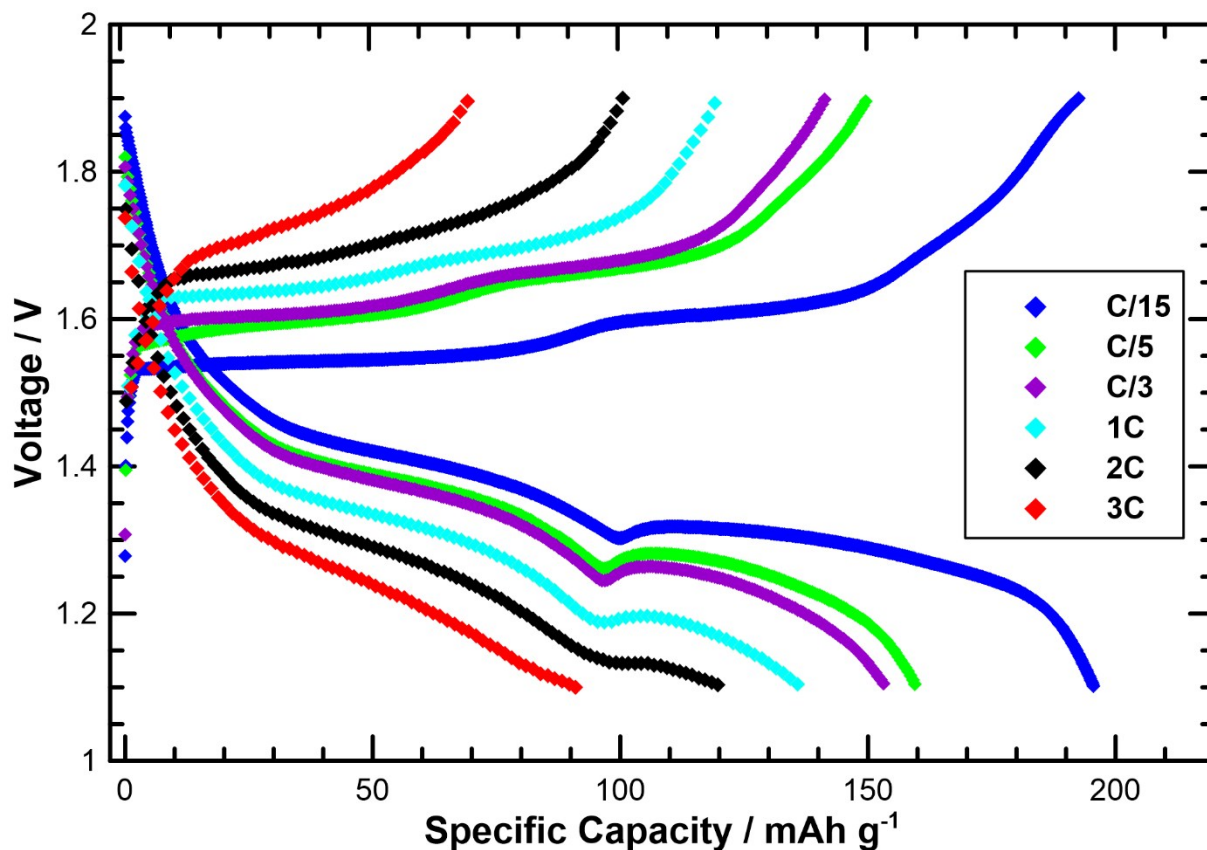
Figure S3. Voltage-capacity curves for charge and discharge steps at different C rates of MnO_2/ 2 M $ZnSO_4$ / Zn cell. The curves at the fifth cycle of every C rate (from Figure 2a, Main text) are shown.
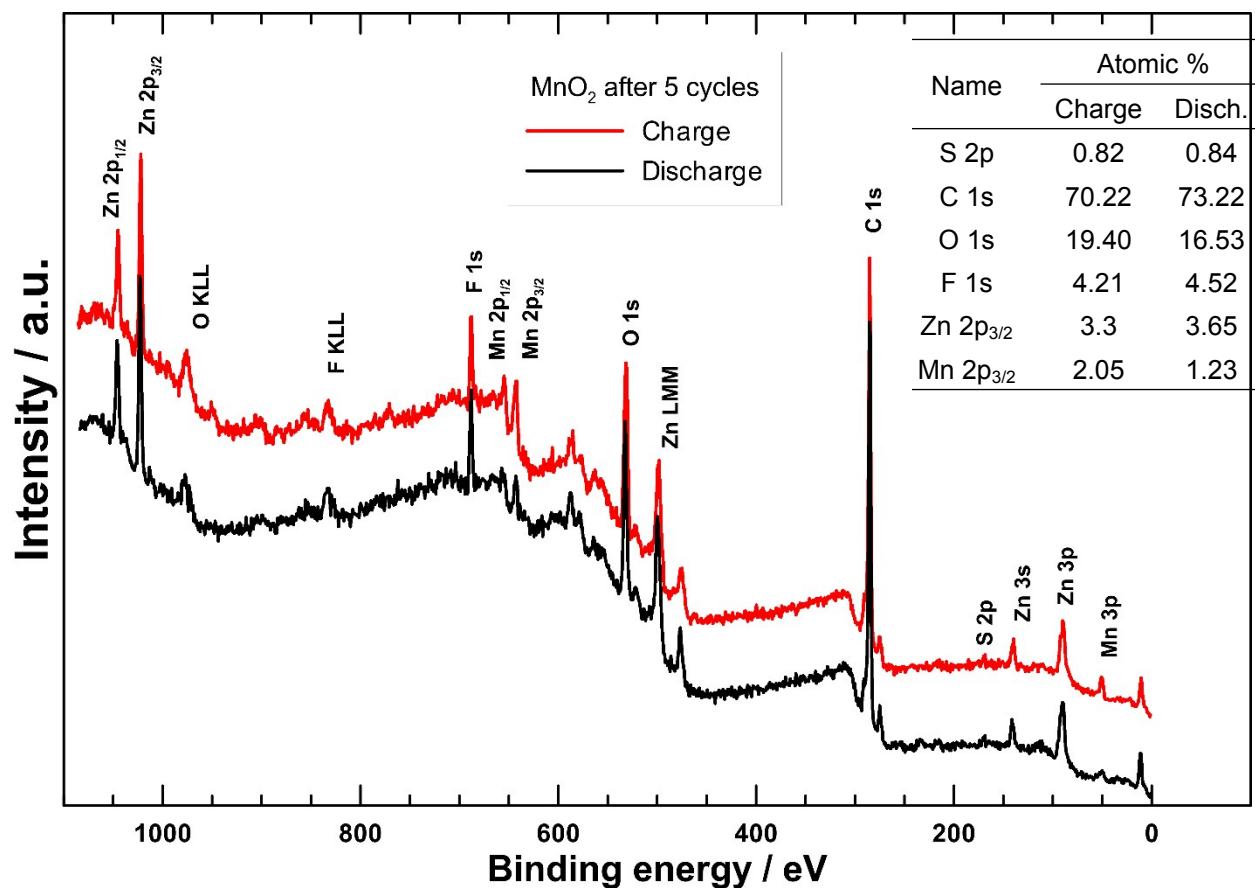
Two distinct processes that were discussed, and are most pronounced at the C/15 rate, can be divided into two segments: the first segment covers the initial 100 mAh g^{-1} capacity and the second segment covers specific capacities higher than 100 mAh g^{-1} (Figure S3). It can be observed that the second discharge segment becomes less pronounced at higher C rates and almost completely disappears at the highest rate (3C), while the first segment almost retains the same capacity at all C rates examined. With higher rates of discharge, polarizations losses (kinetic, ohmic and diffusion) become more significant. The ohmic loss at the highest C rate is ~10 mV, thus can be completely neglected. Therefore, kinetic and/or diffusion resistance(s) are more pronounced for the second process. Very similar findings have been reported by Wang et al.[2] who have assigned the faster step to the proton insertion/deinsertion, while the rate dependent one assigned to Zn intercalation/deintercalation. We have confirmed Zn ion activity in this potential range (Figure S7b) and discussed the nature of Zn (de)incorporation (discussion below Table S2).
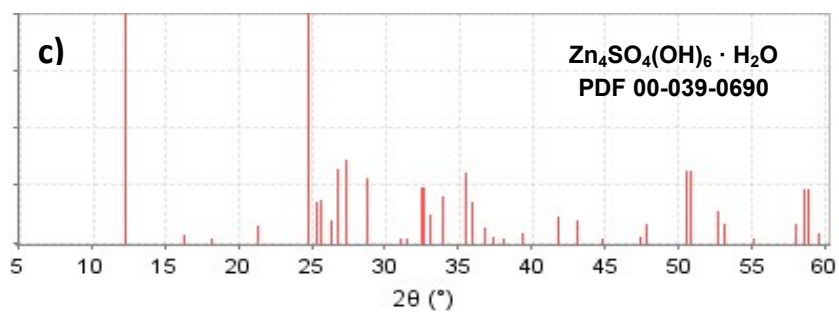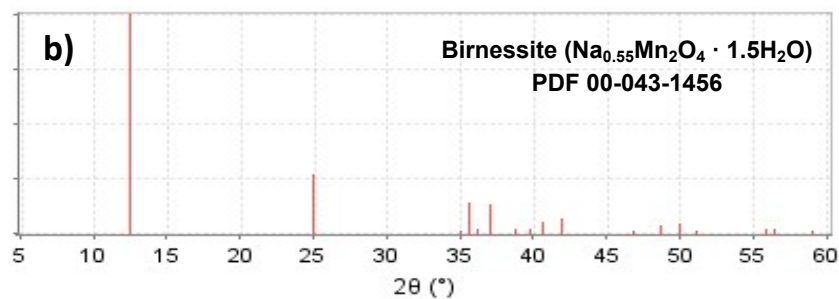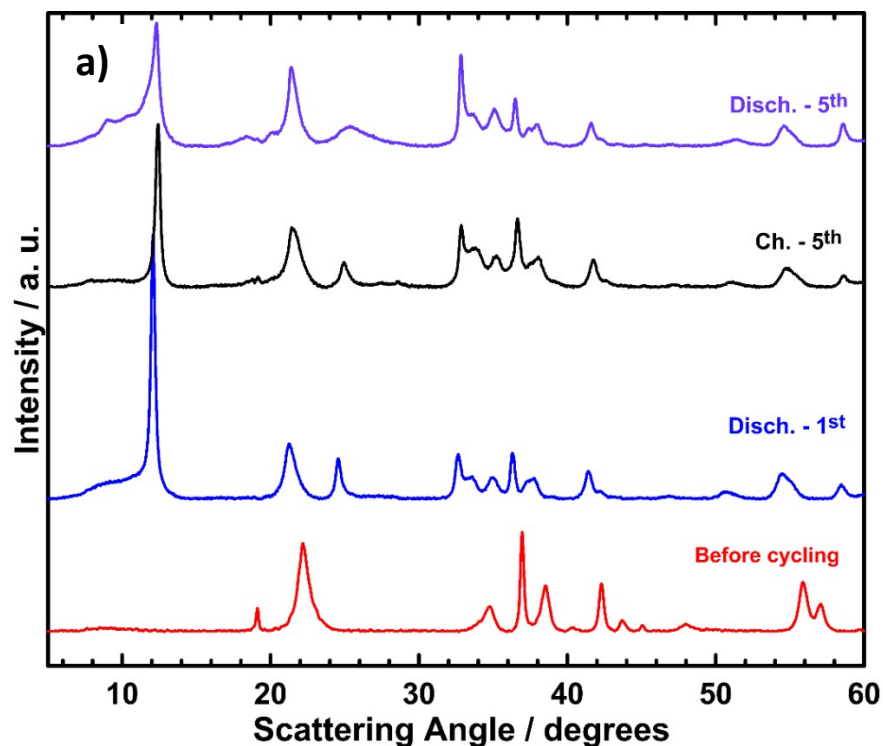
Figure S4. a) Ex-situ XRD patterns of synthesized MnO_2 before and after cycling in 2 M $ZnSO_4$ electrolyte, b) XRD pattern of birnessite phase (PDF 00-043-1456), and c) XRD pattern of Zinc Sulfate Hydroxide Hydrate (PDF 00-039-0690).

Three major features can be observed when XRD patterns of before and after cycling are compared. The first observation is that the ramsdellite phase does not undergo significant

structural changes but only some minor changes in the lattice parameters can be observed. Secondly, the minor spinel phase disappears completely, and thirdly new Bragg peaks appear at 2θ values of 7-9°, 12°, 24.5°, 33°, 51° and 59°. The most intense peak at the scattering angle of 12° and the reflection at 24.5° could be assigned to $Zn_4SO_4(OH)_6 \cdot H_2O$ (zinc sulphate hydroxide hydrate, PDF 00-039-0690) or birnessite, δ-MnO_2, (PDF 00-043-1456) since both compounds have similar XRD patterns with the most intensive peaks at 12° and 24.5° (Figures S4b and S4c). However, XPS analysis (Figure S5) of the cycled samples in both, the charged and discharged states, revealed that the atomic ratio of Zn to S is approximately 4 to 1, which corresponds to $Zn_4SO_4(OH)_6 \cdot H_2O$. This finding, as well as a better matching of the 51° scattering peak allow us to positively identify the presence of $Zn_4SO_4(OH)_6 \cdot H_2O$. Based on XRD data, Oh et al. reported Zn-birnessite formation[3], but in a later publication they reported that the Zn-buserite phase is formed during discharge and later transforms into the birnessite phase after the electrode is exposed to air and has dried[4]. Chemical precipitation of $Zn_4SO_4(OH)_6 \cdot xH_2O$ in MnO_2/$ZnSO_4$/Zn cells has been already observed[5] and studied in detail by Oh et al.[6]. The authors reported that this phase tend to form throughout the $ZnSO_4$ solution during the charging process because of pH increase in the electrolyte.

Name	Atomic %	
	Charge	Disch.
S 2p	0.82	0.84
C 1s	70.22	73.22
O 1s	19.40	16.53
F 1s	4.21	4.52
Zn 2p$_{3/2}$	3.3	3.65
Mn 2p$_{3/2}$	2.05	1.23

MnO$_2$ after 5 cycles
— Charge
— Discharge

Figure S5. XPS spectra of MnO$_2$ electrodes after 10 cycles in 2 M ZnSO$_4$ and the surface chemical compositions obtained.

In both, charged and discharged states, a significant amount of Zn is present (compared to Mn). In the charged state the atomic ratio of Zn to S is approximately 4 to 1, which corresponds to formation of Zn$_4$SO$_4$(OH)$_6 \cdot$ H$_2$O. In the discharged state the Zn concentration is somewhat higher (Zn : S = 4.3 : 1), however, the excess amount of Zn (the amount remaining after accounting for the Zn amount required for the formation of Zn$_4$SO$_4$(OH)$_6 \cdot$ H$_2$O) is within the limits of the experimental uncertainties. This means that Zn intercalation in MnO$_2$ cannot be claimed with high certainty.
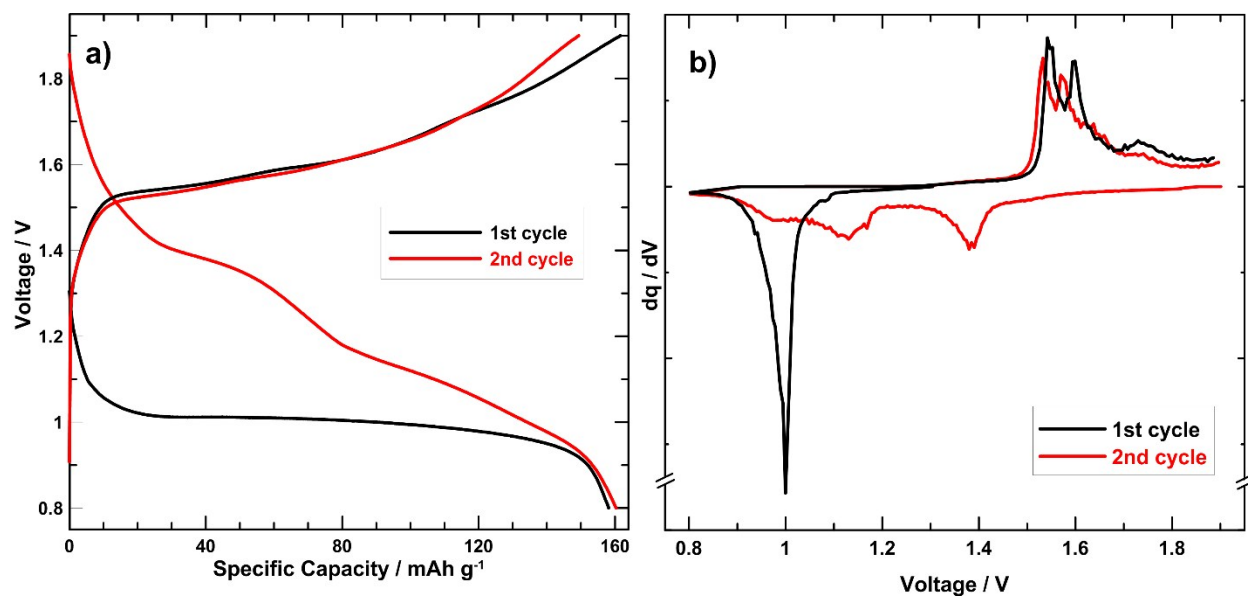
Figure S6. MnO_2/Zn-triflate/Zn cell performance at 100 mA g^{-1}: a) Discharge/charge voltage-capacity curves of first two cycles at 100 mA g^{-1}, and b) Corresponding dq/dV plots.

Table S1. Surface chemical composition of MnO_2 electrodes at the 1st charge and the 2nd discharge state determined by XPS. Electrodes were electrochemically cycled in the MnO_2/Zn-triflate/Zn cells.

Name	Atomic %	
	Charge	Disch.
C 1s	85.44	83.79
O 1s	10.19	10.58
F 1s	1.78	2.52
Zn 2p$_{3/2}$	0.77	1.38
Mn 2p$_{3/2}$	0.48	0.48
Si 2p	1.34	1.25

Table S2. Chemical composition of MnO_2 electrodes, cycled in the MnO_2/Zn-triflate/Zn cells and stopped at the charged and discharged state. Concentrations determined by ICP-OES were transformed to the atomic ratios of Mn, Zn and S.

Name	Atomic ratio	
	Charge	Disch.
Zn	0.5	0.8
Mn	1.0	1.0
S	0.0	0.0

From the ICP and XPS measurements (Tables S1 and S2), the presence of Zn in the cathode in both the charged and discharged states is confirmed. No sulfur is detected by both techniques, thus excluding the possibility of the Zn-triflate salt precipitation. A part of this Zn-containing species was deposited irreversibly, probably chemically, while the reversible formation (between charge and discharge) is ascribed to electrochemical cycling, which is confirmed by very reversible cycling of MnO_2 in an aprotic electrolyte (Figure S7a), giving specific capacity of 50 mAh g^{-1}. Cycling in the aprotic electrolyte provides strong evidence that Zn ions partially contribute to the overall charge storage mechanism.

By comparing total (ICP-OES, Table S2) and surface (XPS, Table S1) composition it is clear that Zn is more abundant at the surface than in the bulk of the cathode. Furthermore, the chemical composition of the surface (Table S1) shows that Zn-containing compounds are preferably formed at the surface during the discharge process. However, it is difficult to distinguish whether a surface process or bulk intercalation into the MnO_2 structure is dominant. For example, Cabana et al.[7] have detected formation of Zn species (ZnO and $Zn_2Mn_3O_8$) as separate particles from those of Mn-oxide at the cathode surface during discharge. Based on this evidence, the authors have excluded Zn intercalation as a dominant process of charge storage mechanism in the highly crystalline spinel phase of MnO_2 in the conditions attempted.

Differential profiles of voltage capacity curves in the Zn-salt based aprotic electrolyte (Figure S7b) reveals that major electrochemical activity of Zn occurs at approximately 0.9 V vs. Zn^{2+}/Zn which corresponds to the smallest peak of the dq/dV curves obtained for MnO_2 cycled in the Zn-triflate water based electrolyte (Figure S6b, second cycle). Although the major activity occurs at 0.9 V, a part of the capacity is gained at the higher potentials, up to 1.2 V vs. Zn^{2+}/Zn; however, in this potential range activity is much less pronounced than in the water electrolyte and no distinct peak

can be observed. This is in agreement with the conclusion from the previous discussion about the C-rate effect on the voltage capacity curves (Figure S3) that Zn incorporation in the cathode occurs at lower potentials.
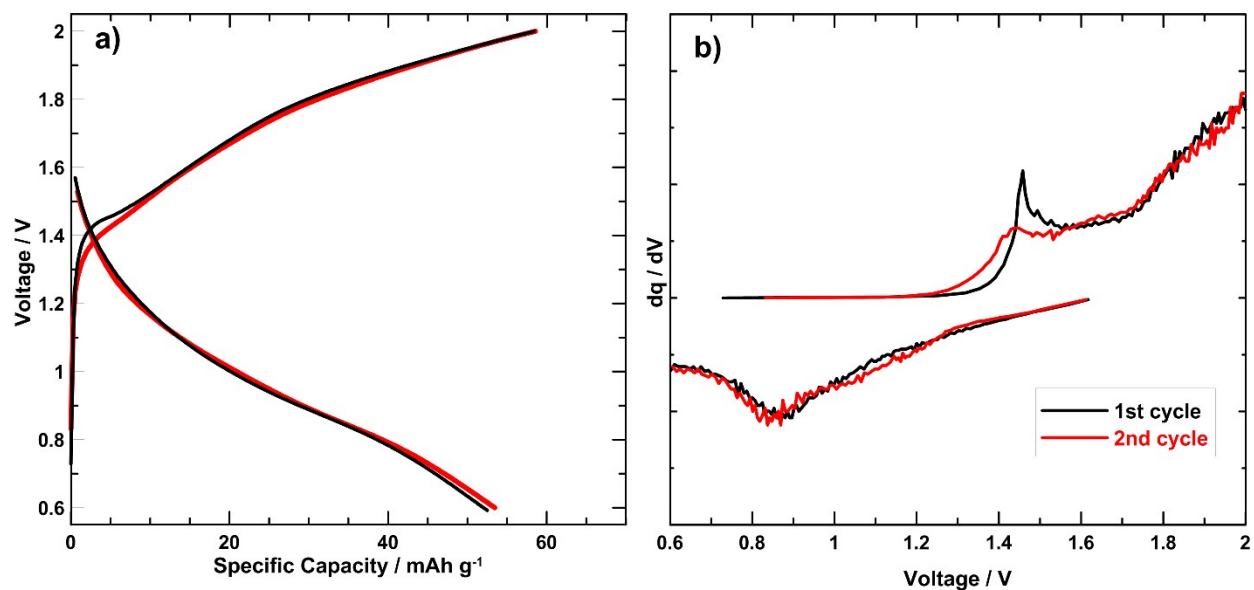
Figure S7. MnO$_2$/Zn-triflate/Zn cell with aprotic electrolyte (0.5 M Zn-triflate, dissolved in acetonitrile) cycled at 100 mA g^{-1}: a) Discharge/charge voltage-capacity curves of first two cycles at 100 mA g^{-1}, and b) Corresponding dq/dV plots.

References

1   Y. Chabre and J. Pannetier, *Prog. Solid State Chem.*, 1995, **23**, 1–130.

2   W. Sun, F. Wang, S. Hou, C. Yang, X. Fan, Z. Ma, T. Gao, F. Han, R. Hu, M. Zhu and C. Wang, *J. Am. Chem. Soc.*, 2017, **139**, 9775–9778.

3   B. Lee, C. S. Yoon, H. R. Lee, K. Y. Chung, B. W. Cho and S. H. Oh, *Sci. Rep.*, 2015, **4**, 6066.

4   B. Lee, H. R. Lee, H. Kim, K. Y. Chung, B. W. Cho and S. H. Oh, *Chem. Commun.*, 2015, **51**, 9265–9268.

5   S. H. Kim and S. M. Oh, *J. Power Sources*, 1998, **72**, 150–158.

6   B. Lee, H. R. Seo, H. R. Lee, C. S. Yoon, J. H. Kim, K. Y. Chung, B. W. Cho and S. H. Oh, *ChemSusChem*, 2016, **9**, 2948–2956.

7   M. G. Nolis, A. Adil, H. D. Yoo, L. Hu, R. D. Bayliss, S. H. Lapidus, L. Berkland, P. J. Phillips, J. W. Freeland, C. Kim, R. F. Klie and J. Cabana, *J. Phys. Chem. C*, 2018, **122**, 4182–4188.